Photochemical Synthesis of H_2O_2 from the $H_2O\cdots O(^3P)$ van der Waals Complex: Experimental Observations in Solid Krypton and Theoretical Modeling

Susanna Pehkonen,[†] Kseniya Marushkevich,[†] Leonid Khriachtchev,[†] Markku Räsänen,*[,†] Bella L. Grigorenko,[‡] and Alexander V. Nemukhin[‡]

Department of Chemistry, University of Helsinki, P.O. Box 55 (A.I.Virtasen aukio 1), Helsinki FIN-00014, Finland, and Department of Chemistry, M.V. Lomonosov Moscow State University, 1/3 Leninskie Gory, Moscow 119992, Russian Federation

Received: July 5, 2007; In Final Form: August 31, 2007

Productive photochemical synthesis of hydrogen peroxide, H_2O_2, from the $H_2O\cdots O(^3P)$ van der Waals complex is studied in solid krypton. Experimentally, we achieve the three-step formation of H_2O_2 from H_2O and N_2O precursors frozen in solid krypton. First, 193 nm photolysis of N_2O yields oxygen atoms in solid krypton. Upon annealing at ∼25 K, mobile oxygen atoms react with water forming the $H_2O\cdots O$ complex, where the oxygen atom is in the triplet ground state. Finally, the $H_2O\cdots O$ complex is converted to H_2O_2 by irradiation at 300 nm. According to the complete active space self-consistent field modeling, hydrogen peroxide can be formed through the photoexcited $H_2O^+-O^-$ charge-transfer state of the $H_2O\cdots O$ complex, which agrees with the experimental evidence.

1. Introduction

Hydrogen peroxide has both scientific and industrial values. In the atmosphere, hydrogen peroxide provides an important link between gas-phase radicals and aqueous chemistry, and it plays a significant role in many atmospheric oxidation reactions. The only known gas-phase source of tropospheric H_2O_2 is the reaction between two HO_2 radicals producing H_2O_2 and O_2.[1] As a source of atmospheric aqueous phase H_2O_2, gas-to-liquid partitioning of gas-phase H_2O_2 and aqueous photoformation have been considered.[2] H_2O_2 has been observed on the surface of Europa.[3] Molecular complexes of atmospheric constituents strongly affect atmospheric chemistry and physics.[4] The low-frequency intermolecular vibrations are important channels for the absorption of both solar radiation that enters the atmosphere and the outgoing infrared (IR) surface radiation.[5,6]

In our previous studies on H_2O_2 photochemistry in low-temperature rare-gas matrices, we have demonstrated that hydrogen peroxide decomposes by UV light producing the $H_2O\cdots O(^3P)$ complex as one of the two photolysis products, and that this complex can be photochemically converted back to H_2O_2.[7−9] We tentatively proposed a mechanism that involved photoinduced charge-transfer between H_2O and $O(^3P)$ with a concomitant recombination to H_2O_2. The vibrational bands of $H_2O\cdots O(^3P)$ were observed at 3730.1 and 3633.0 cm^{-1} in solid argon, at 3718.6 and 3622.4 cm^{-1} in solid krypton, and at 3704.3 and 3607.3 cm^{-1} in solid xenon. No other bands were observed for this species. The assignment was based on isotopic substitution, selective photoinduced processes between H_2O_2 and $H_2O\cdots O$, and ab initio calculations.[8] Interaction between water and oxygen atoms is of atmospheric chemistry interest,[10] and the proposed photoreaction might be an additional source of hydrogen peroxide in practical environment. In the gas phase, the reaction between H_2O and $O(^1D)$ produces two OH radicals but not H_2O_2.[1] In agreement, theoretical calculations on $H_2O(X^1A_1) + O(^1D)$ reaction showed that the main reaction channel (OH + OH) corresponded to a pathway with negligible energy barrier.[11] On the other hand, photolysis of the H_2O/O_3 mixture in solid argon produced hydrogen peroxide, indicating a reaction between H_2O and $O(^1D)$.[12] Irradiation of water ice by UV light, ions, and electrons produces hydrogen peroxide, and other species such as O_2, H_2, and HO_2.[13] Moore and Hudson irradiated ice by H^+ protons at 16 K and also observed the formation of hydrogen peroxide.[14] The authors suggested that H_2O_2 arises from a recombination reaction of two OH radicals. In solid Xe, formation of H_2O_2 was observed upon 193 nm photolysis of water dimers.[15]

Mobility of oxygen atoms in solid environment is an important phenomenon, and it has been extensively investigated theoretically and experimentally.[16−27] The experimental studies cover both photoinduced and thermal mobility processes. Danilychev and Apkarian used the $O(^3P) + O(^3P)$ recombination reaction to investigate mobility of oxygen atom in free-standing crystals of krypton and xenon.[16] Oxygen atoms were generated from 193 nm photolysis of O_2 or N_2O, and their mobility was characterized as long-range mobility. The Rg−O (Rg = Ar, Kr, or Xe) pair potentials were also described theoretically.[16] In solid argon, Meyer and Metzger observed that diffusion of oxygen atoms was very slow at 20 K but already significant at 33 K.[19] Thermoluminescence of NO_2 in solid argon, an indication of the NO + O reaction and oxygen atom diffusion, was visible already at 9 K.[20] In free-standing crystals of xenon and in xenon matrices, Benderskii and Wight observed a thermally activated recombination reaction of $O + O_2$ to occur at 14−25 K in a time scale of 10^2-10^5 s.[21] This was most probably short-range mobility, because long-range (global) mobility of O atoms in solid xenon proceeded above 27 K.[22] Short-range mobility of atoms in solid environment corresponds to lower activation energies as compared to long-range (global) mobility.[23]

* Corresponding author. E-mail: markku.rasanen@helsinki.fi.
[†] University of Helsinki.
[‡] M.V. Lomonosov Moscow State University.

10.1021/jp075233s CCC: $37.00
Published on Web 10/19/2007

An essential novel feature of the present work is that we demonstrate efficient and controlled photochemical synthesis of hydrogen peroxide in samples, which do not initially contain H_2O_2. More specifically, we study photochemical formation of H_2O_2 in solid krypton from the environmentally important precursors H_2O and N_2O. Oxygen atoms are generated by UV photolysis of N_2O and then thermally mobilized, which leads to the $H_2O\cdots O$ complex. The $H_2O\cdots O$ complex is then photochemically converted to H_2O_2.

To explain the experimental observations, we carried out quantum chemical calculations of the structures that can be formed along the reaction coordinate. We examined fairly large areas on the triplet-state and singlet-state potential energy surfaces, including geometry optimization in the excited states, with the wavefunctions constructed in the complete active space self-consistent field (CASSCF) approximation.[28] The energies of the critical points along the reaction coordinate were then recomputed by using the perturbation theory corrections to the CASSCF energies. These quantum calculations show that the experimentally observed photochemical transformations are consistent with the possible flows along the potential energy surfaces.

2. Experimental Section

2.1. Experimental Setup. Two glass bulbs were filled with ~400 Torr of krypton (99.997% purity, AGA). The N_2O/Kr ratio in one bulb was varied from 1:50 to 1:1000, the typical ratio being 1:700 (N_2O of technical grade, AGA). A drop of liquid deionized and distilled water was added into the second bulb and degassed before filling with krypton. This water-containing bulb was used as a source of constant H_2O/Kr composition (H_2O/Kr = 1/16) determined by the vapor pressure of water at room temperature and the partial pressure of krypton. The two bulbs were connected to the matrix deposition line through calibrated leak valves (Leybold, Varian), and the gases were mixed in the line before the deposition port. The N_2O/H_2O/Kr mixture was deposited onto a CsI substrate kept at 25 K in a closed-cycled helium cryostat (APD, DE 202A) and then cooled to 8.5 K. Using the known integrated absorptivities[29] and integrated intensities of the N_2O and H_2O bands, the typical N_2O/H_2O/Kr ratio in the prepared matrix was approximately 1/1/700. The matrix thickness varied between 70 and 100 μm. The infrared spectra (4000−650 cm^{-1}) were recorded with a Fourier transform infrared (FTIR) spectrometer (Nicolet 60 SXB) with spectral resolution of 1.0 or 0.25 cm^{-1}. Typically 200 interferograms were coadded. Photolysis of N_2O was carried out with an excimer laser (MSX-250, MPB Technologies Inc.) operating at 193 nm (ArF) with a typical pulse energy density of 10 mJ/cm^2. Frequency-doubled radiation from an optical parametric oscillator (OPO Sunlite, Continuum) was used at 300 nm with a typical pulse energy of 6 mJ and a beam diameter of ~15 mm.

2.2. Experimental Results. The measured infrared (IR) spectrum of N_2O in solid Kr showed the following features. In the 4000−650 cm^{-1} region, two fundamental vibrations were found at wavenumbers of 2220.6 cm^{-1} (ν_3) and 1283.7 cm^{-1} (ν_1) (see Figure 1). The ν_2 fundamental (588.0 cm^{-1} in the gas phase)[30a] was blocked by the detector window. Additionally, several overtone and combination bands of N_2O were observed at 3477.2 ($\nu_1+\nu_3$), 2791.3 ($\nu_2+\nu_3$), 2561.0 ($2\nu_1$), 1875.4 ($\nu_1+\nu_3$), and 1160.4 cm^{-1} ($2\nu_2$). All of these bands agree well with previous measurements in argon, xenon, and nitrogen matrices and in the gas phase.[30] For the H_2O/Kr mixture, the bands at 3765.6, 3747.7, and 3700.7 cm^{-1} (see Figure 1) in the OH stretching region and the bands at 1652.0, 1621.0, and 1605.9 cm^{-1} in the OH bending region belong to monomeric water as characterized by Engdahl and Nelander.[31] In some cases, a minor amount of dimeric water was observed with bands at 3569.3 and 1591.3 cm^{-1}.[31]

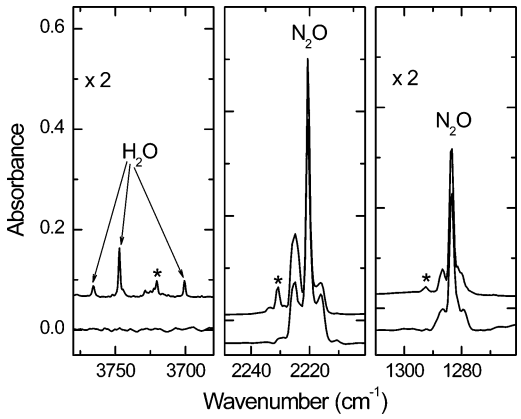

Figure 1. IR spectrum of $N_2O\cdots H_2O$ (upper spectrum) and N_2O (lower spectrum) in solid krypton. Bands marked with a star belong to the $N_2O\cdots H_2O$ complex. Monomeric water and nitrous oxide absorptions are marked in the figure. The spectra were measured at 8.5 K.

When N_2O and H_2O are mixed in solid krypton, new absorption bands appear in both the N_2O and the H_2O regions. Relative amounts of N_2O and H_2O were varied to distinguish the $N_2O\cdots H_2O$ complex absorption bands. Comparing the H_2O/Kr, N_2O/Kr, and N_2O/H_2O/Kr experiments, the following complex absorptions bands can be distinguished: 3720.5 cm^{-1} in the OH stretching region, 1591.1 cm^{-1} in the OH bending region of H_2O, 2227.2 cm^{-1} in the N_2O (ν_3) region, and 1292.6 cm^{-1} in the N_2O (ν_1) region. The IR spectra of N_2O/Kr and N_2O/H_2O/Kr matrices complex are presented in Figure 1. The observed $N_2O\cdots H_2O$ absorption in the N_2O (ν_3) region is in good agreement with a previous gas-phase study.[32] According to our knowledge, there are no previous matrix-isolation studies on the $N_2O\cdots H_2O$ complex. In the main series of experiments, we tried to minimize the amount of the $N_2O\cdots H_2O$ complex; that is, the samples were essentially monomeric with respect to N_2O and water. However, a minor amount of $N_2O\cdots H_2O$ complex is always present, as seen in Figure 2a.

In Figure 2b, the difference spectrum represents the result of 193 nm photolysis. Photolysis at 193 nm efficiently decomposes N_2O in solid krypton, whereas the concentration of H_2O is practically unchanged. In Figure 2b, the negative peaks at 3765.5 and 3700.7 cm^{-1} and positive peak at 3747.7 cm^{-1} belong to different rotational transitions of monomeric water. The concentration of monomeric water is not changed; this was verified by integrating the areas and summing up the three bands. The observed changes in the monomeric water absorption intensities are due to the known spin conversions.[33] After photolysis, no IR active products, for instance, NO, N_2O_2, or O_3, are detected. The only photolysis channel of N_2O is to form molecular nitrogen and atomic oxygen in analogy with the gas phase and solid-state results on N_2O.[16,34]

Upon annealing of a photolyzed sample at ≥14 K, new absorptions appear at 3718 and 3623 cm^{-1} (see the difference spectrum in Figure 2c). These bands belong to the $H_2O\cdots O$ complex, which was identified previously as a product of UV photolysis of hydrogen peroxide in solid rare-gases.[8] In Figure 2c, the spectrum after the photolysis is used as a background to view the changes taking place in annealing. The amount of monomeric water decreases upon annealing featuring its reaction with mobile oxygen atoms. Ozone is formed in small amounts

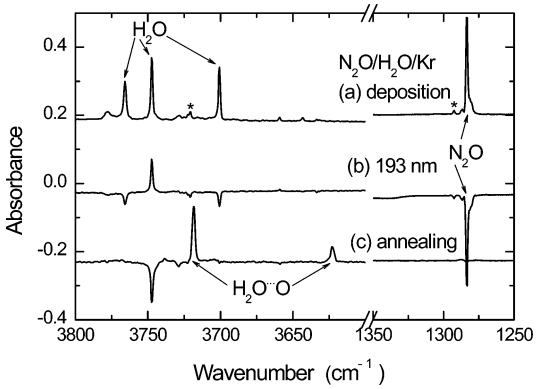

Figure 2. Photolysis and annealing of $H_2O/N_2O/Kr$ (1/1/700) matrix. (a) IR spectrum of as-deposited $N_2O/H_2O/Kr$ matrix. A minor amount of $N_2O\cdots H_2O$ complex is present, marked with a star. (b) Difference spectrum with respect to spectrum (a) showing the results of 193 nm photolysis. The intensity changes of the monomeric water bands are due to spin conversion (see ref 33). No change of the H_2O concentration occurs at this stage. (c) Difference spectrum with respect to spectrum (b) showing the result of annealing at temperatures $\geq$14 K. The H_2O concentration decreases at this stage. The spectra were measured at 8.5 K.

and especially above 25 K (1033.6 cm^{-1}). For the $H_2O\cdots O$ complex formation, we distinguished two stages as seen in Figure 3a. The first stage occurs at 14−18 K, and it is presumably a reaction between H_2O and O fragments, which are in close vicinity to each other. The second stage is seen above 22 K, and it is a reaction where oxygen atom globally moves further from its original site. This activation temperature of global oxygen-atom mobility agrees with the previous results.[9,16] The kinetics of the "global" (higher-temperature) reaction was studied as follows. First, a sample was annealed at 21 K for several minutes, which finishes the short-range process. Second, the sample was annealed at 22−25 K to study the global oxygen mobility. Finally, the sample was annealed to 28 K to finalize the processes connected with mobile oxygen atoms, and the integrated area of the 3718 cm^{-1} band at this temperature was used for normalization of the kinetic curves. The curves are presented in Figure 3b. Above 25 K, the formation of the $H_2O\cdots O$ complex is very fast, and the formation kinetics cannot be practically measured. Natural logarithm of the characteristic time (in minutes) of the formation of the $H_2O\cdots O$ complex as a function of reciprocal annealing temperature is presented in Figure 3c. The characteristic time corresponds to 0.63 level of the $H_2O\cdots O$ concentration measured after annealing to 28 K. Linear fit to this data yields an Arrhenius type activation energy of about (70 $\pm$ 6) meV (550 cm^{-1}) for the mobility of O atoms.

Upon 300 nm photolysis, the $H_2O\cdots O$ complex absorptions decrease and the H_2O_2 absorptions appear and increase at 3574.3 and 3583.7 cm^{-1}, as seen in the difference spectrum in Figure 4a, and in the bending region at 1268.7 and 1274.0 cm^{-1}.[44] In Figure 4a, the spectrum after annealing is used as a background to view the changes taking place upon the 300 nm photolysis. The changes in the intensities of the monomeric water absorptions at 3765.6, 3747.7, and 3700.7 cm^{-1} are due to spin conversion.[33] The areas of the strongest ν_6 band of H_2O_2 (1268.7 cm^{-1}) and the 3718 cm^{-1} band of $H_2O\cdots O$ absorptions were integrated giving the relative concentrations as a function of irradiation time (see Figure 4b). Irradiation of the $H_2O\cdots O$ complex at 193 nm also produces H_2O_2, but in smaller amounts, because formation of H_2O_2 is less efficient at this wavelength and H_2O_2 is efficiently decomposed by 193 nm to OH radicals

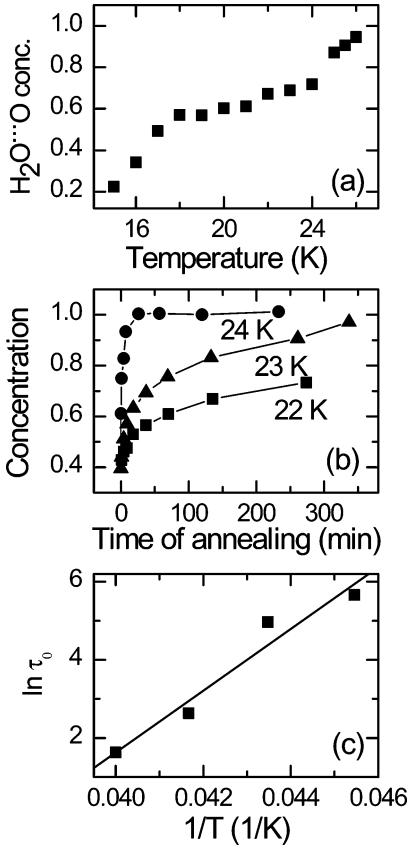

Figure 3. (a) Formation of the $H_2O\cdots O$ complex as a function of annealing temperature. The temperature was increased with the 1 K/min rate, and the spectra were measured at the elevated temperatures. Short-range ($\geq$14 K) and long-range ($\geq$22 K) formation of the $H_2O\cdots O$ complex can be distinguished. Before annealing, the $N_2O/H_2O/Kr$ = 1/1/700 matrix was photolyzed by 193 nm. The $H_2O\cdots O$ concentrations were obtained by integration of the 3718 cm^{-1} band, which were normalized by the value obtained after additional annealing to 28 K for ~10 min. The spectra were measured at 8.5 K. (b) Kinetic curves of the formation of $H_2O\cdots O$ complex at various annealing temperatures. (c) Characteristic time (in minutes) for the formation of $H_2O\cdots O$ as a function of the annealing temperature. The averaged slope gives activation energy of ~70 meV.

as described elsewhere.[7−9] At 300 nm, H_2O_2 is not decomposed significantly.

2.3. Discussion of Experimental Results. Mobility of oxygen atoms in solid state has been a subject of many studies; however, the precise diffusion mechanism is not fully understood. According to the previous models,[16] mobile oxygen atoms are in the triplet ground state. The simulations resulted in activation barriers of 0.15−0.17 eV for $O(^3P)$[26] and 0.82−0.87 eV for $O(^1D)$ mobility.[18] Danilychev and Apkarian suggested a mechanism according to which a crossing between the triplet and singlet states occurs that facilitates mobility of oxygen atoms.[16] Our estimates for such activation energy of (70 $\pm$ 6) meV (550 cm^{-1}) are somewhat lower than the computational results in ref 26 and agree better with the experimental site dependent activation energies (0.05 and 0.13 eV) obtained by Danilychev and Apkarian.[18] We believe that more careful theoretical work can improve the agreement between theoretical and experimental data. In fact, this was demonstrated for H atom diffusion in solid xenon.[35] Theoretical modeling of O atom solvation and diffusion exceeds the scope of the present work.

The reaction between H_2O and mobile O atoms producing the $H_2O\cdots O$ complex is firmly demonstrated experimentally. The $H_2O\cdots O$ complex is formed upon annealing above 14 K.

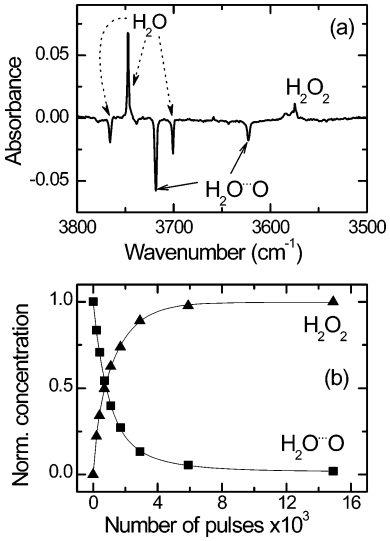

Figure 4. (a) Formation of H_2O_2 from $H_2O\cdots O$ upon irradiation of 300 nm, a difference spectrum, where the spectrum after annealing is used as a background. The changes of the monomeric water band intensities are due to spin conversion.[33] No change of the H_2O concentration occurs. (b) Formation of H_2O_2 and decomposition of $H_2O\cdots O$ as a function of 300 nm irradiation time. The ν_6 band of H_2O_2 (1268.7 cm^{-1}) and the 3718 cm^{-1} band of $H_2O\cdots O$ were used for integration the band areas.

The formation efficiency of the $H_2O\cdots O$ complex in our experiments is independent of the time between the end of photolysis and the beginning of annealing in a time scale of 0−3 h. This observation confirms that mobile oxygen atoms are in the triplet ^3P state. This is an important fact because 193 nm photolysis of N_2O yields singlet state oxygen atoms,[34] and the $O(^1D)$ lifetime is 110−115 s in the gas phase.[36] In solid SF_6, the $O(^1D)$ lifetime is 780 ms.[24] Furthermore, if oxygen atoms were in the singlet state, we would expect them to react with water as observed by Schriver et al. in solid argon[12] and in ices.[37] Another possibility is a formation of the $H_2O\cdots O(^1D)$ complex, the so-called oxywater, which computationally is found stable,[38] but has not been observed experimentally. According to the calculations, oxywater reorganizes to H_2O_2 with a barrier of 0.25 eV.[10] These observations and calculations support our assertion that the oxygen atoms in our experiment react with water in the triplet ^3P state.

Hydrogen peroxide in this study is formed in the photochemical reaction $H_2O\cdots O \xrightarrow{h\nu} H_2O_2$. We compared the amount of photolyzed N_2O and formed H_2O_2 by integrating the corresponding IR absorption bands and using the known band intensities [300.7 km mol^{-1} for the ν_3 band of N_2O (2220.6 cm^{-1}) and 60 km mol^{-1} for the ν_6 band of H_2O_2 (1268.7 cm^{-1})].[29] The estimation shows that 50−60% of oxygen atoms from decomposed N_2O are transferred to H_2O_2, which is a very high yield. In addition, a small part of oxygen atoms may react with each other or O_2 impurities to produce O_3, which is observed as a minor product at 1033.6 cm^{-1}. Formation of O_2 in similar experiments was found previously.[9]

In summary, the experimental synthesis of hydrogen peroxide consists of the following steps:

$$N_2O \xrightarrow{193nm} N_2 + O(^1D) \quad (1)$$

$$O(^1D) \xrightarrow{\Delta t} O(^3P) \quad (2)$$

$$O(^3P) + H_2O \xrightarrow{\text{annealing}} H_2O\cdots O \quad (3)$$

$$H_2O\cdots O \xrightarrow{h\nu} H_2O_2 \quad (4)$$

All species are solvated in solid krypton. The quantum chemistry modeling described below refers to the latest step of H_2O_2 photoformation.

3. Modeling

3.1. Computational Details. Scans over potential energy surfaces have been performed by using the complete active space self-consistent field (CASSCF) method.[28] Two orbitals correlating to the oxygen 1s atomic orbitals were kept doubly occupied in all configuration state functions, while 12 active orbitals were available for partial occupation of 14 electrons. This selection of the active space allowed us to describe qualitatively correct all species occurring in the photochemical reactions ($H_2O\cdots O$, $OH\cdots OH$, H_2O_2) in the triplet and singlet states. The basis sets were of the aug-cc-pVTZ quality with the s- and p-type diffuse functions on all atoms. Unconstrained geometry optimizations in the various parts of the triplet and singlet state potential surfaces were performed in the CASSCF approximation, and the energies in the points of the major interest were recomputed by using the second-order multiconfigurational quasi-degenerate perturbation theory (MC-QDPT2) as implemented in the GAMESS[39] or PC GAMESS[40] programs. An accurate theoretical treatment of the $H_2O\cdots O$ complex is more computationally demanding than that of the hydrogen peroxide molecule. However, to maintain a uniform level for the required description of chemical transformations from $H_2O\cdots O$ to H_2O_2, we applied the same computational scheme for all species occurring along the reaction path.

3.2. Computational Results. First, we compare structural, spectral, and energetic results obtained in this work with the available experimental and computational data. The equilibrium geometry parameters of the ground-state hydrogen peroxide are provided as Supporting Information in Table S1. Previous CASSCF calculations of Liu et al.[41] predicted the values very similar to ours, while more advanced methodology used by Watts and Francisco[42] allowed the authors to obtain the geometry parameters that almost coincided with the gas-phase experimental estimates.[42] Beyond the 0.02 Å discrepancy in the O−O distance, our results seem to be fairly accurate. The equilibrium geometry of the $H_2O\cdots O$ complex in the triplet state is shown in Figure 5. This structure is similar to the results reported previously in ref 8 using the UMP2/6-311++G(2d,-2p) approximation.

In Table 1, we show the computed harmonic frequencies and the observed bands of the $H_2O\cdots O$ complex in argon and in

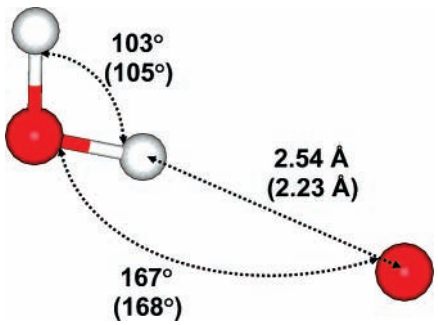

Figure 5. Optimized structure of the planar $H_2O\cdots O(^3P)$ complex. Geometry parameters in parentheses are from ref 8 as computed in the UMP2/6-311++G(2d,2p) approximation.

TABLE 1: Calculated and Observed Vibrational Frequencies of $H_2O\cdots O$ (cm^{-1})

mode	ref (8)	this work (unscaled)[a]	this work (scaled by 0.97)	experimental (Ar)[b]	experimental (Kr)[b]
ν_1	105	110 (1.16)			
ν_2	167	154 (2.82)			
ν_3	241	282 (2.82)			
ν_4	1708	1702 (1.37)			
ν_5, OH stretching	3850	3794 (0.16)	3680	3633	3622
ν_6, OH stretching	3972	3899 (1.48)	3782	3731	3719

[a] This work; IR intensities in D^2/amu·$Å^2$ are given in parentheses. [b] Reference 8.

TABLE 2: Computed Vertical Excitation Energies of H_2O_2 (eV)

excitation	MCQDPT2 (CASSCF geometry)[a]	CASPT2 (CASSCF geometry)[b]	EOM-CCSD (QCISD geometry)[c]	gas-phase exp.[d]
S0−S1	5.66	5.49	5.99	
S0−S2	6.62	6.69	7.94	
S0−T1		4.40		
S1−S2	0.96	1.2	1.95	1.3

[a] This work. [b] Reference 41. [c] Reference 42. [d] Reference 45.

krypton matrices. For comparison, the calculated and experimental frequencies for hydrogen peroxide are presented in the Supporting Information in Table S2. As generally accepted, we applied the scaling procedure to account for anharmonic and matrix effects. The scaling factor used here (0.97) was selected to demonstrate a reasonable correspondence of the computed harmonic frequencies of the OH vibrations in the van der Waals complex OH···OH [3640 and 3654 cm^{-1} (triplet state)] with bands of the OH radical measured in argon and krypton (3554, and 3547, 3542, 3539 cm^{-1}, respectively).[7−9]

Table 2 shows the computed vertical excitation energies of H_2O_2. Our MCQDPT2 energy calculations at the CASSCF geometry configuration allow us to obtain the results close to the values reported in ref 41 (multireference CASSCF second-order perturbation theory at the CASSCF geometry). The data of Table 2 apparently illustrate the difficulties in the theoretical estimates of excited-state energies. Indeed, a more advanced calculation procedure of ref 42 does not show better agreement with the experimental data than the approaches used by Liu et al. and in the present work. We may expect typical errors of up to 0.5 eV in computing the excitation energies in this particular application. From all of these comparisons, we conclude that the present computational strategy provides a qualitatively correct description of the system.

The diagram shown in Figure 6 summarizes the possible transformations in the H_2O_2 system. Initially, the system presents

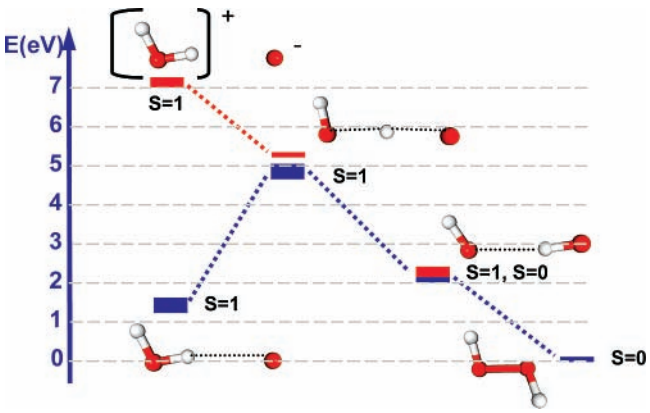

Figure 6. Energy diagram for the photoreaction connecting the triplet state of $H_2O\cdots O$ and the singlet state of H_2O_2.

the water-oxygen complex $H_2O\cdots O(^3P)$ in the triplet state shown in the lower left corner. Without imposing symmetry constraints in the calculation procedure, its energy is triply degenerate (due to components of the P state of the oxygen atom) as shown by the thick stick in the diagram. The fourth triplet state corresponds to the excited state of the complex $H_2O^+\cdots O^-$ (^3P). The computed vertical excitation energy, 5.8 eV, was obtained when averaging over four states in the CASSCF procedure followed by the multiconfiguration quasi-degenerate second-order perturbation theory (MCQDPT2) calculations. This gas-phase value agrees with the semiempirical estimate, 5.35 eV, obtained in ref 7 by using the equation:

$$E^{tr} = IP(H_2O) - EA(O) - U(Re) - E^{sol} \qquad (5)$$

The value for the isolated species should be corrected by taking into account matrix solvation and possible errors in computations of excited-state energy. In particular, we can obtain the experimental value for the excitation energy in the argon matrix (4.84 eV or 256 nm) if we combine the solvation energy estimated in ref 7 as 0.51 eV, and a reasonable computational error of 0.5 eV as discussed above. The experimental excitation profile for the $H_2O\cdots O \rightarrow H_2O_2$ recovery shifts to longer wavelengths when moving from argon to krypton matrix.[9] This small red shift can be interpreted within the charge-transfer model by taking into account the change in the solvation energy due to a larger dielectric constant of krypton.[9] Thus, the energetic scale of the species in the left part of the diagram is fairly consistent with the experimental results. It shows that the excitation of about 5 eV of the water-oxygen complex in the matrix allows one to reach the charge-transfer $H_2O^+\cdots O^-$ state.

Other states shown in Figure 6 were obtained as follows. We performed an unconstrained geometry optimization in the CASSCF approximation for the fourth triplet state starting from the geometry configuration of the ion-pair $H_2O^+\cdots O^-$ (^2P) complex. As a result of descent along this potential energy surface, we arrived to the structure shown in the diagram as the HO···H···O species. We did not locate a precise structure corresponding to the conical intersection of the surfaces, but found a point where the energies of all four roots are almost degenerate. Starting from this geometry of the HO···H···O complex, we switched the optimization procedure to the first triplet state. The unconstrained energy optimization for the lowest triplet state allowed us to arrive to the van der Waals complex of two OH radicals as illustrated in the diagram. At this point, the energies of the triplet and singlet states are almost degenerate, and, therefore, we explored the potential energy surface of the lowest singlet state starting from this point. The rearrangement from the van der Waals complex of two OH radicals to the hydrogen peroxide molecule can be easily accomplished in solid environment. Therefore, we conclude that hydrogen peroxide can be produced in the matrix from the photoexcited $H_2O^+\cdots O^-$ water-oxygen complex.

4. Concluding Remarks

We demonstrated the formation of H_2O_2 from the H_2O and N_2O precursors using photoexcitation of the $H_2O\cdots O$ complex at 300 nm in solid krypton. The $H_2O\cdots O$ complex was formed in a reaction of thermally mobilized triplet state O atoms and water molecules. In turn, the O atoms solvated in solid krypton were generated by 193 nm photolysis of N_2O. Thus, H_2O_2 was synthesized by UV light and thermal treatment from matrix-isolated H_2O and N_2O in solid environment. The yield of the synthesis of H_2O_2 exceeds 50% with respect to decomposed N_2O. The proposed mechanism for the $H_2O\cdots O \rightarrow H_2O_2$ photoreaction assumes involvement of the $H_2O^+\cdots O^-$ charge-transfer. In particular, this mechanism is consistent with the simple energetic estimates (ref 7) and observed matrix shift of the excitation spectrum.[9]

The experimental conclusions are supported by the CASSCF quantum chemistry calculations. First, the energy of light-induced charge-transfer state of $H_2O^+\cdots O^-$ as compared to $H_2O\cdots O$ is consistent with the experimental observations (about 5 eV). Second, the reorganization of $H_2O^+\cdots O^-$ to H_2O_2 is energetically probable, and it involves the $HO\cdots H\cdots O$ and $HO\cdots HO$ species. The present theory is a compromise between relative simplicity and adequate description. We believe that our computational method provides qualitatively correct results. The accuracy of computations can be improved using a more sophisticated level of theory; however, this exceeds the scope of the present research.

The present results show that the $H_2O\cdots O \rightarrow H_2O_2$ photoreaction can occur in the gas and in solid phases. The present photoreaction can serve as an additional source of H_2O_2 in the atmosphere.

Acknowledgment. The work was supported by the Academy of Finland partially through CoE CMS. K.M. acknowledges a research grant from the Magnus Ehrnrooth foundation. The Russian team acknowledges partial support from the Federal Scientific and Technical Program (Grant 2006-RI-112.0/001/052).

Supporting Information Available: Equilibrium ground-state parameters of H_2O_2 (Table S1) and the calculated and experimental frequencies (Table S2) of H_2O_2. This material is available free of charge via the Internet at http://pubs.acs.org.

References and Notes

(1) Finlayson-Pitts, B. J.; Pitts, J. N., Jr. *Chemistry of the Upper and Lower Atmosphere*; Academic Press: San Diego, CA, 2000.

(2) Anastasio, C.; Faust, B. C.; Allen, J. M. *J. Geophys. Res.* **1994**, *99*, 8231−8248.

(3) Carlson, R. W.; Anderson, M. S.; Johnson, R. E.; Smythe, W. D.; Hendrix, A. R.; Barth, C. A.; Söderblom, L. A.; Hansen, G. B.; McCord, T. B.; Dalton, J. B.; Clark, R. N.; Shirley, J. H.; Ocampo, A. C.; Matson, D. L. *Science* **1999**, *283*, 2062−2064.

(4) *Molecular Complexes in Earth's, Planetary, Cometary and Interstellar Atmospheres*; Vigasin, A. A., Slanina, Z., Eds.; World Scientific: Singapore, 1998.

(5) Salby, M. L. *International Geophysics Series, Vol. 61*; Academic Press: San Diego, CA, 1996.

(6) Svishchev, I. M.; Boyd, R. J. *J. Phys. Chem. A* **1998**, *102*, 7294−7296.

(7) Khriachtchev, L.; Pettersson, M.; Tuominen, S.; Räsänen, M. *J. Chem. Phys.* **1997**, *107*, 7252−7259.

(8) Pehkonen, S.; Pettersson, M.; Lundell, J.; Khriachtchev, L.; Räsänen, M. *J. Phys. Chem. A* **1998**, *102*, 7643−7648.

(9) Khriachtchev, L.; Pettersson, M.; Jolkkonen, S.; Pehkonen, S.; Räsänen, M. *J. Chem. Phys.* **2000**, *112*, 2187−2194.

(10) Sennikov, P. G.; Ignatov, S. K.; Schrems, O. *ChemPhysChem* **2005**, *6*, 392−412 and references therein.

(11) Sayós, R.; Oliva, C.; Gonzáles, M. *J. Chem. Phys.* **2001**, *115*, 8828−8837.

(12) Schriver, L.; Barreau, C.; Schriver, A. *Chem. Phys.* **1990**, *140*, 429−438.

(13) Zheng, W.; Jewitt, D.; Kaiser R. I. *Astrophys. J.* **2005**, *639*, 534−548 and references therein.

(14) Moore, M. H.; Hudson, R. L. *Icarus* **2000**, *145*, 282−288.

(15) Khriachtchev, L.; Tanskanen, H.; Pettersson, M.; Räsänen, M.; Ahokas, J.; Kunttu, H.; Feldman, V. *J. Chem. Phys.* **2002**, *116*, 5649−5656.

(16) Danilychev, A. V.; Apkarian, V. A. *J. Chem. Phys.* **1993**, *99*, 8617−8627.

(17) Lawrence, W. G.; Apkarian, V. A. *J. Chem. Phys.* **1992**, *97*, 2229−2236.

(18) Danilychev, A. V.; Apkarian, V. A. *J. Chem. Phys.* **1994**, *100*, 5556−5566.

(19) Meyer, B.; Metzger, J. L. *J. Chem. Phys.* **1974**, *60*, 796−798.

(20) Fournier, J.; Deson, J.; Vermeil, C. *J. Chem. Phys.* **1977**, *67*, 5688−5690.

(21) Benderskii, A. V.; Wight, C. A. *J. Chem. Phys.* **1996**, *104*, 85−94.

(22) Kiviniemi, T.; Pettersson, M.; Khriachtchev, L.; Räsänen, M.; Runeberg, N. *J. Chem. Phys.* **2004**, *121*, 1839−1848.

(23) Khriachtchev, L.; Pettersson, M.; Pehkonen, S.; Isoniemi, E.; Räsänen, M. *J. Chem. Phys.* **1999**, *111*, 1650−1657.

(24) Mohammed, H. H. *J. Chem. Phys.* **1990**, *93*, 412−415.

(25) Ning, X.-J.; Qin, Q.-Z. *J. Chem. Phys.* **2001**, *114*, 9969−9974.

(26) Ford, M. B.; Foxworthy, A. D.; Mains, G. J.; Raff, L. M. *J. Phys. Chem.* **1993**, *97*, 12134−12143.

(27) Schriever, U.; Hebert, T.; Kolb, D. M. *Ber. Bunsen-Ges Phys. Chem.* **1992**, *96*, 1032−1037.

(28) *Computational Molecular Spectroscopy*; Jensen, P., Bunker, P., Eds.; Wiley, 2000.

(29) (a) Galapov, B. S.; Dudev, T. T. *Vibrational Intensities*; Elsevier: Amsterdam, 1996; p 185. (b) N_2O: Toth, R. A. *Appl. Opt.* **1991**, *32*, 7326−7365. (c) H_2O_2: Perrin, A V.; Flaud, J.-M.; Camy-Peyret, C.; Schriver, L.; Schriver, A.; Arcas, P. H. *J. Mol. Spectrosc.* **1995**, *171*, 358−373.

(30) (a) In the gas phase: Begun, G. M.; Fletcher, W. H. *J. Chem. Phys.* **1957**, *28*, 414−418. (b) In solid N_2: Lapinski, A.; Spanget-Larsen, J.; Waluk, J.; Radziszewski, J. G. *J. Chem. Phys.* **2001**, *115*, 1757−1764. (c) In Xe and in Ar: Lawrence, W. G.; Apkarian, V. A. *J. Chem. Phys.* **1992**, *97*, 2224−2228.

(31) Engdahl, A.; Nelander, B. *J. Mol. Spectrosc.* **1989**, *193*, 101−109.

(32) Gimmler, G.; Havenith, M. *J. Mol. Spectrosc.* **2002**, *216*, 315−321.

(33) Redington, R. L.; Milligan, D. E. *J. Chem. Phys.* **1963**, *39*, 1276−1284.

(34) Adams, S. F.; DeJoseph, C. A., Jr.; Carter, C. C.; Miller, T. A.; Williamson, J. M. *J. Phys. Chem. A* **2001**, *105*, 5977−5983.

(35) Khriachtchev, L.; Tanskanen, H.; Pettersson, M.; Räsänen, M.; Feldman, V.; Sukhov, F.; Orlov, A.; Shestakov, A. *J. Chem. Phys.* **2002**, *116*, 5708−5716.

(36) Bhardwaj, A.; Haider, S. A. *Adv. Space Res.* **2002**, *29*, 745−750.

(37) Chaabouni, H.; Schriver-Mazzuoli, L.; Schriver, A. *Low Temp. Phys.* **2000**, *26*, 712−718.

(38) (a) Huang, H. H.; Xie, Y.; Schaefer, H. F., III. *J. Phys. Chem.* **1996**, *100*, 6076−6080. (b) Xie, Y.; Allen, W. D.; Yamaguchi, Y.; Shaefer, H. F., III. *J. Chem. Phys.* **1996**, *104*, 7615−7623.

(39) Schmidt, M. W.; Baldridge, K. K.; Boatz, J. A.; Elbert, S. T.; Gordon, M. S.; Jensen, J. H.; Koseki, S.; Matsunaga, N.; Nguyen, K. A.; Su, S. J.; Windus, T. L.; Dupuis, M.; Montgomery, J. A. *J. Comput. Chem.* **1993**, *14*, 1347−1363.

(40) Nemukhin, A. V.; Grigorenko, B. L.; Granovsky, A. A. *Moscow State Univ. Res. Bull. Khimia* **2004**, *45*, 75−102.

(41) Liu, Y.-J.; Persson, P.; Lunell, S. *Mol. Phys.* **2004**, *102*, 2575−2584.

(42) Watts, J. D.; Francisco, J. S. *J. Chem. Phys.* **2006**, *125*, 104301−104309.

(43) (a) Koput, J. *J. Mol. Spectrosc.* **1986**, *115*, 438−441. (b) Comes, F. J.; Gericke, K. H.; Grunewald, A. U.; Klee, S. *Ber. Bunsen-Ges. Phys. Chem.* **1988**, *92*, 273−281.

(44) Pettersson, M.; Tuominen, S.; Räsänen, M. *J. Phys. Chem. A* **1997**, *101*, 1166−1171.

(45) Grunewald, A. U.; Gericke, K.-H.; Comes, F. J. *J. Chem. Phys.* **1987**, *87*, 5709−5721.